JOURNAL OF GEOPHYSICAL RESEARCH

Supporting Information for: Mesoscale Ocean Processes: The Critical Role of Stratification in the Icelandic Region

Charly de Marez [1], Clara R. Vives [2], Esther Portela Rodriguez[3],

Angel Ruiz Angulo [1]

[1]University of Iceland, Reykjavík, Iceland

[2]Globe Institute, Section for Geobiology, University of Copenhagen, Denmark

[3]Univ Brest, CNRS, IRD, Ifremer, Laboratoire d'Océanographie Physique et Spatiale, Plouzané, France

1. High resolution numerical modelling

To confirm that the turbulence properties observed in SWOT data are independent from the altimetric measurement process, we compute an SSH variance estimate in a high resolution numerical model. We use outputs from a realistic numerical simulation conducted as part of the GIGATL set of Atlantic Ocean simulations (Gula et al., 2021), using the Coastal and Regional Ocean COmmunity model (CROCO), a version of the ROMS model (Shchepetkin & McWilliams, 2005). This model solves the hydrostatic primitive equations using the full equation of state for seawater (Shchepetkin & McWilliams, 2011). Specifically, we use the GIGATL1 version with a horizontal resolution of 1 km and 100 terrain-following levels, which ensure to solve the mesoscale dynamics up to the Northern edge of our domain of interest. For more details on the simulation, and validations, we refer the reader to previous studies (Ruan et al., 2021; Barkan et al., 2021; Qu et al., 2021; Mashayek et al., 2021; Vic et al., 2022; Uchida et al., 2022; Tagliabue et al., 2022; Schubert et al., 2023; Napolitano et al., 2024). Similarly as in SWOT observations, very weak SSH signal is seen in the simulation north of Iceland . This goes along with a very weak turbulence field, as seen in the surface relative vorticity (Fig. S1b). We estimate the SSH wavenumber spectra for the month of May in the simulation in two squared areas north and south, by computing first frequency-wavenumber spectra, and then averaging over frequencies and azimuthally. This compares favourably with SWOT; (1) the spectrum computed south as twice the amplitude of the spectrum north, and (2) the slope of the spectrum is similar in both region and is ~ 5; see Fig. S1c.

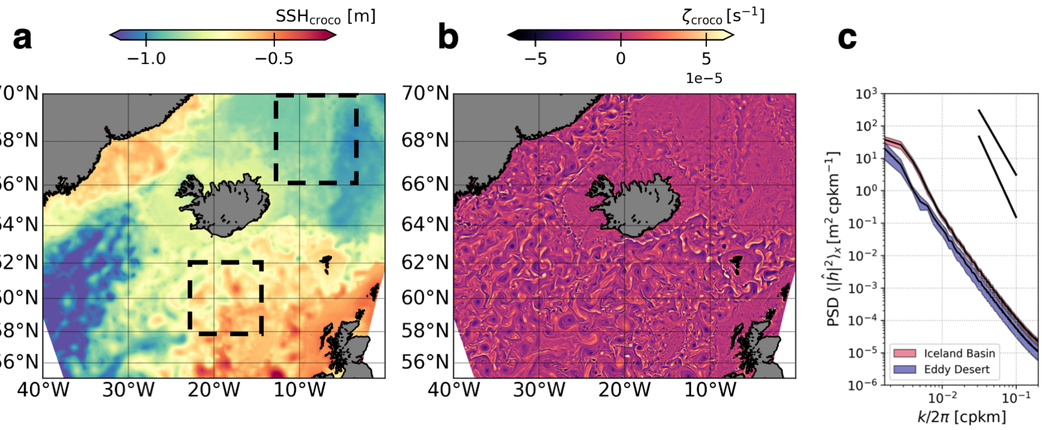

Figure S1. (a, resp. b) SSH (resp. surface relative vorticity) snapshot from high resolution CROCO simulation in May; dashed lines show the —squared— areas considered to compute the spectra shown in panel c. (c) Same as Fig. 4b in the Iceland Basin and the "eddy desert" (south and north of Iceland, respectively) using the month of May in the CROCO simulation

2. Surface forcings

To check the surface forcings in our aera of interest, we compute the monthly and daily averages of wind stress τ norm from a Global Ocean Hourly Sea Surface Wind and Stress product (`doi.org/10.48670/moi-00305`, downloaded using E.U. Copernicus Marine Service Information). It contains hourly Level-4 sea surface wind and stress fields at 0.125 degrees horizontal spatial resolution obtained from Scatterometer observations. Monthly averaged net heat flux Q_{net} is obtained from ECCO re-analysis (V4r4 ECCO, see a full description of the model in Fukumori et al., 2021).

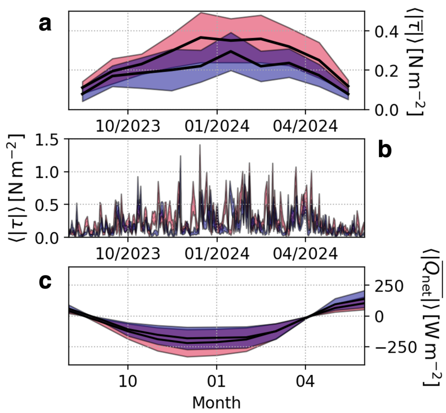

Figure S2. (a) Monthly averaged wind stress norm north (blue) and south (red) of Iceland. (b) Daily averaged wind stress, and (c) Monthly averaged net heat flux.

3. Vertical sections of biogeochemical properties from BGC-Argo floats

We display here examples of the timeseries before vertical integration from BGC-Argo floats.

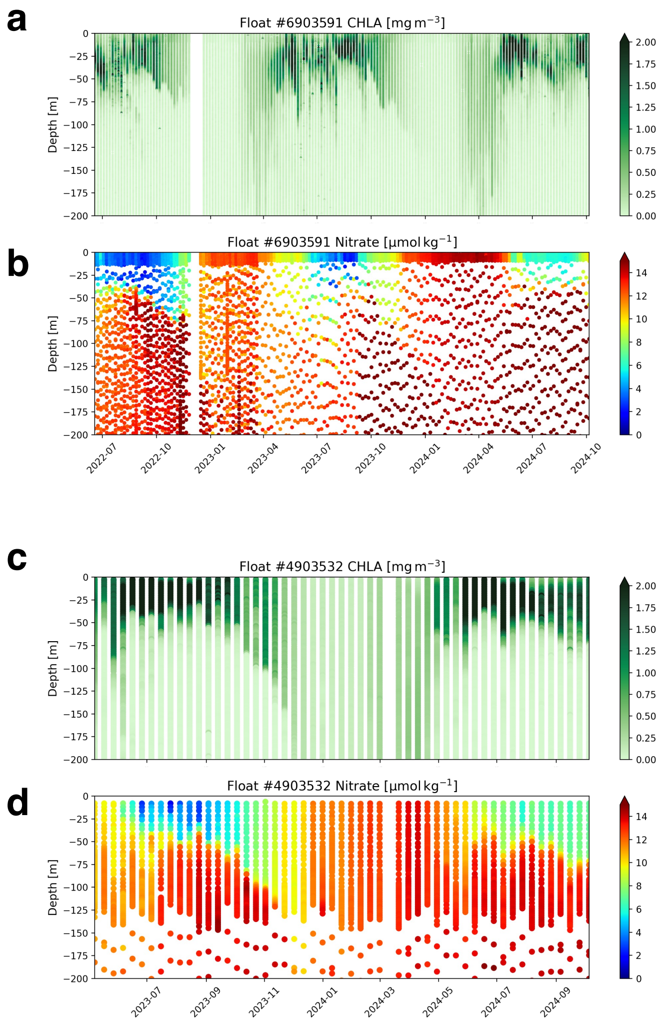

Figure S3. (a, resp. b) Timeseries of chlorophyll-a (resp. nitrate) from BGC-Argo float #6903591 (northern region). (c,d) Same as panels a,b for float #4903532 (southern region).

4. Nitrate concentration timeseries from BGC-Argo. floats

We display here timeseries of nitrate measurements-related quantities

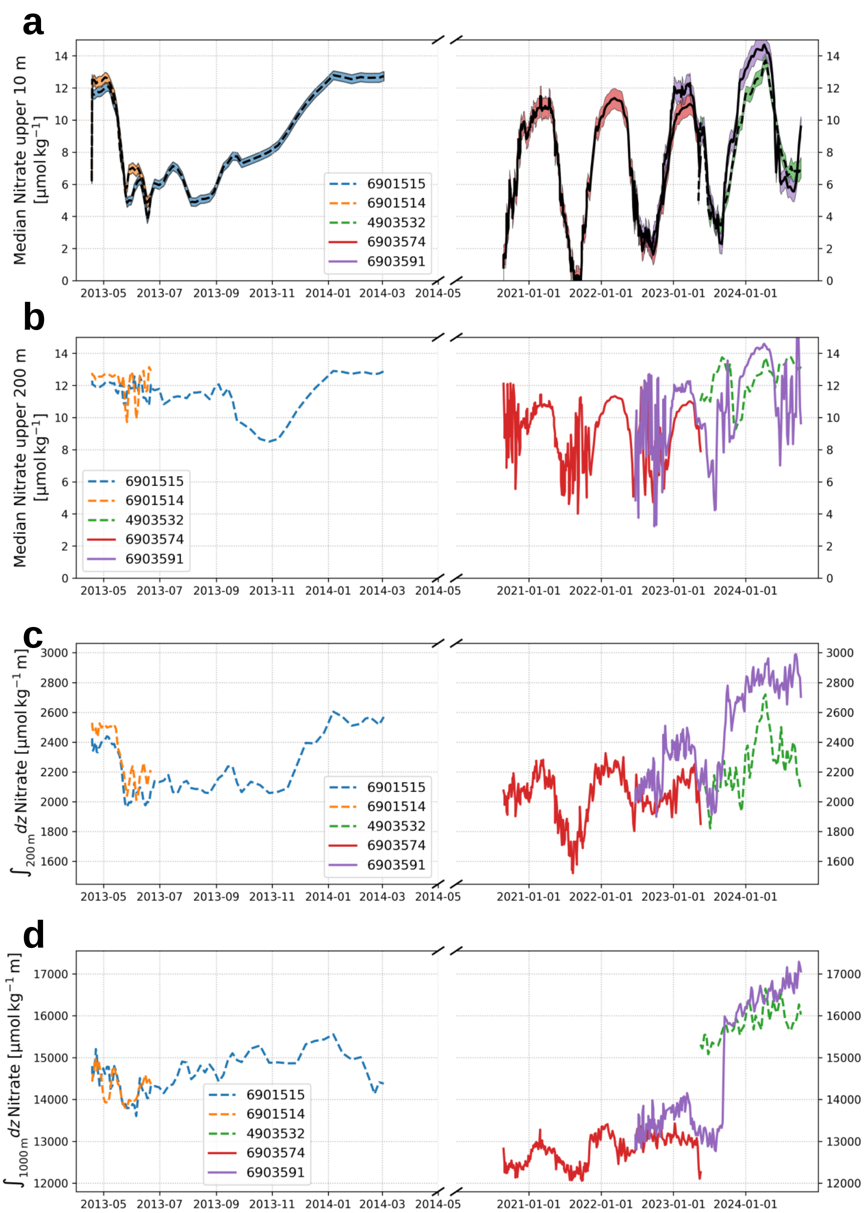

Figure S4. (a) Timeseries of median value of nitrate in the upper 10 m for the same BGC-Argo floats as in panel a; envelopes show the median incertitude. (b) Same as panel a but in the first upper 200 m. (c, resp. d) timeseries of vertically integrated nitrate concentration in the upper 200 m (resp. 1000 m) from BGC-Argo floats.

References

Barkan, R., Srinivasan, K., Yang, L., McWilliams, J. C., Gula, J., & Vic, C. (2021). Oceanic mesoscale eddy depletion catalyzed by internal waves. *Geophysical Research Letters*, *48*(18), e2021GL094376.

Fukumori, I., Wang, O., Fenty, I., Forget, G., Heimbach, P., & Ponte, R. M. (2021, February). *Synopsis of the ECCO Central Production Global Ocean and Sea-Ice State Estimate, Version 4 Release 4* (Tech. Rep.). Zenodo. Retrieved 2022-10-25, from `https://zenodo.org/record/3765928` (Version Number: 4 Release 4) doi: 10.5281/ZENODO.3765928

Gula, J., Theetten, S., Cambon, G., & Roullet, G. (2021, June). *Description of the gigatl simulations.* Zenodo. Retrieved from `https://doi.org/10.5281/zenodo.4948523` doi: 10.5281/zenodo.4948523

Mashayek, A., Gula, J., Baker, L., Garabato, A. N., Cimoli, L., & Riley, J. (2021). Mountains to climb: On the role of seamounts in upwelling of deep ocean waters. *Preprint*(Version 1).

Napolitano, D. C., Carton, X., & Gula, J. (2024). Vertical interaction between nbc rings and its implications for south atlantic water export. *Journal of Geophysical Research: Oceans*, *129*(4), e2023JC020741.

Qu, L., Thomas, L., & Gula, J. (2021). Bottom mixing enhanced by tropical storm-generated near-inertial waves entering critical layers in the Straits of Florida. *Geophysical Research Letters*, *48*(15), e2021GL093773.

Ruan, X., Wenegrat, J. O., & Gula, J. (2021). Slippery bottom boundary layers: The loss of energy from the general circulation by bottom drag. *Geophysical Research Letters*, *48*(19), e2021GL094434.

Schubert, R., Vergara, O., & Gula, J. (2023). The open ocean kinetic energy cascade is strongest in late winter and spring. *Communications Earth & Environment*, *4*(1), 450.

Shchepetkin, A. F., & McWilliams, J. C. (2005, January). The regional oceanic modeling system (ROMS): a split-explicit, free-surface, topography-following-coordinate oceanic model. *Ocean Modelling*, *9*(4), 347–404.

Shchepetkin, A. F., & McWilliams, J. C. (2011, January). Accurate Boussinesq oceanic modeling with a practical, "Stiffened" Equation of State. *Ocean Modelling*, *38*(1-2), 41–70. doi: 10.1016/j.ocemod.2011.01.010

Tagliabue, A., Lough, A. J., Vic, C., Roussenov, V., Gula, J., Lohan, M. C., ... Williams, R. G. (2022). Mechanisms driving the dispersal of hydrothermal iron from the northern Mid Atlantic Ridge. *Geophysical Research Letters*, *49*(22), e2022GL100615.

Uchida, T., Le Sommer, J., Stern, C., Abernathey, R., Holdgraf, C., Albert, A., ... others (2022). Cloud-based framework for inter-comparing submesoscale permitting realistic ocean models. *Geoscientific Model Development Discussions*, *2022*, 1–32.

Vic, C., Hascoët, S., Gula, J., Huck, T., & Maes, C. (2022). Oceanic mesoscale cyclones cluster surface Lagrangian material. *Geophysical Research Letters*, *49*(4), e2021GL097488.